Nonlocal Interaction of Inverse Magnetic Energy Transfer in Hall Magnetohydrodynamic Turbulence*)

Keisuke ARAKI and Hideaki MIURA[1)]

Okayama University of Science, Okayama 700-0005, Japan
[1)]*National Institute for Fusion Science, Toki 509-5292, Japan*

(Received 24 December 2010 / Accepted 5 August 2011)

A detailed analysis of forward and inverse energy transfer processes due to the Hall term effect in freely decaying, homogeneous, isotropic Hall magnetohydrodynamics (HMHD) turbulence is performed through Fourier and wavelet analyses. We analyzed three snapshot datasets that were taken from such a period to allow the turbulence to develop sufficiently with a nearly constant magnetic Reynolds number. Because the Fourier energy spectra in these snapshots show remarkable agreement after the normalization in terms of the dissipation rates and the diffusion coefficients, they are considered as a universal equilibrium state. By analyzing the numerical solutions that are generated without any external forcing, it is confirmed that the inverse energy transfer due to the Hall term effect is intrinsic to HMHD dynamics. Orthonormal divergence-free wavelet analysis reveals that nonlinear mode interactions contributing to the inverse energy transfer exhibit a nonlocal feature, while those for the forward transfer are dominated by a local feature.

Keywords: hall magnetohydrodynamics, wavelet analysis, inverse energy transfer, nonlocal interaction

DOI: 10.1585/pfr.6.2401132

1. Introduction

Although single-fluid magnetohydrodynamic (MHD) equations are considered an appropriate platform for studying macroscopic behaviors of fusion plasmas, some phenomena may be outside the scope of these equations. The roles of two-fluid effects have attracted attention in various research areas such as fusion plasmas [1, 2] and astrophysical plasmas [3, 4]. The Hall MHD (HMHD) system is known as a simple fluid model that includes a two-fluid effect.

The difference between the MHD and HMHD systems was discovered to be caused by significant differences in energy dissipation tendencies, structure formation processes, and profiles of the generated coherent structures [5]. In addition, it was discovered that energy transfer of the magnetic field to smaller scales was supressed due to the Hall term effect by comparing the full simulation result of HMHD equations with that of the truncated model [6]. This result suggests that the Hall term effect maintains large scale spatial structures in fully developed turbulence, which is important for plasma confinement.

Despite this distinct difference, we compared the wavelet-scale spectra of the energy exchange due to the induction term and found that the dominance of local energy transfer and energy transfer to small scales were common to both cases [7]. There is no qualitatively significant difference in the profiles of the energy transfer spectra. That is, the Hall term does not directly change the characteristics of the magnetic induction process.

The supression of energy transfer to small scales appears consistent with the backscatter of the magnetic energy. Through Fourier-mode analysis of shell-averaged energy budget equations, energy transfer from the smaller to larger scale components, which Mininni *et al.* discovered that energy transfers from smaller to larger scale components [8]. However, the velocity field is maintained by an ABC flow forcing at the wave number $|k_x| = |k_y| = |k_z| = 2$. Owing to this forcing, energy spectrum and some energy transfer spectra exhibit a somewhat spiky profile at $|\vec{k}| \simeq 3$. The effect of forcing on the generated magnetic field is indirect, and the Hall term effect occurs solely by the magnetic field; therefore, the backscatter phenomenon's effect on HMHD turbulence appears inconclusive.

In our previous work, we employed divergence-free wavelet analysis to confirm that backscattering due to the Hall term effect exists and that energy is mainly transferred to the modes very close in spatial scale for all spatial resolution classes; that is, the entire energy transfer process occurs locally [7]. However, because only one snapshot dataset was previously analyzed [7], further study is necessary to achieve a firm understanding.

2. Numerical Method

In the present study, we focus on the time development of a nonlinear magnetic energy transfer caused by the Hall term effect. To exclude the influence of forcing, we analyze

author's e-mail: araki@are.ous.ac.jp

*) This article is based on the presentation at the 20th International Toki Conference (ITC20).

a freely decaying, homogeneous, isotropic turbulence of the incompressible HMHD system, which is calculated by Miura and Hori [5]. The incompressible HMHD equations are given by

$$\frac{\partial \boldsymbol{u}}{\partial t} + (\boldsymbol{u}\cdot\nabla)\boldsymbol{u} = -\nabla P + \boldsymbol{j}\times\boldsymbol{b} + \nu\nabla^2\boldsymbol{u}\,, \tag{1}$$

$$\frac{\partial \boldsymbol{b}}{\partial t} = \nabla\times((\boldsymbol{u}-\epsilon\boldsymbol{j})\times\boldsymbol{b}) + \eta\nabla^2\boldsymbol{b}\,, \tag{2}$$

where $\boldsymbol{u}$ is the bulk velocity field and satisfies $\nabla\cdot\boldsymbol{u} = 0$, $\boldsymbol{b}$ is the magnetic field, $\boldsymbol{j} := \nabla\times\boldsymbol{b}$ is the current density field, P is the total pressure, ν is the kinematic viscosity, η is the resistivity, and ϵ is the parameter for the relative strength of the Hall term.

The parameters are set to $\nu = \eta = 1\times10^{-3}$ and $\epsilon = 0.05$. The number of grid points for calculation is $N^3 = 512^3$. The pseudospectral method with 2/3 dealiasing rule is adopted ($k_{\max} = 170$). The details of numerical schemes and initial conditions are described in Ref. [5]. We analyzed three snapshot datasets at the time $t = 1.0$, 1.5, 2.0, which are referred to as $2T_0$, $3T_0$, and $4T_0$, respectively, in Ref. [9]. These snapshot datasets were taken at a time interval that is sufficiently after the period at which the amplitudes of the vorticity and current density fields achieved their maximum values ($t = 0.5$, see Fig. 1 (b) of Ref. [9]). As is shown in Fig. 1 (c) of Ref. [9], the time development of the Taylor microscale Reynolds number and its magnetic counterpart were rather settled for $t \gtrsim 1.0$. In particular, the Reynolds number of the magnetic field was almost constant ($R^M_{\lambda'} \simeq 93$). Hence, it is strongly expected that the characteristics of these three snapshot datasets reflect some universal features of spontaneously generated HMHD turbulence.

The velocity and magnetic fields are decomposed into Fourier and orthonormal divergence-free wavelet modes as follows:

$$\boldsymbol{f}(\vec{x},t) = \sum_{\vec{k}} \boldsymbol{f}(\vec{k};\vec{x},t) = \sum_j \boldsymbol{f}_j(\vec{x},t)\,, \tag{3}$$

where

$$\boldsymbol{f}(\vec{k};\vec{x},t) := \widehat{\boldsymbol{f}}(\vec{k},t)\exp\left(i\vec{k}\cdot\vec{x}\right), \tag{4}$$

$$\boldsymbol{f}_j(\vec{x},t) := \sum_{\epsilon}\sum_{\vec{l}}\sum_{\sigma} f_{j\epsilon\vec{l}\sigma}(t)\,\boldsymbol{\psi}_{j\epsilon\vec{l}\sigma}(\vec{x})\,, \tag{5}$$

and $\boldsymbol{f}$ stands for $\boldsymbol{u}$ or $\boldsymbol{b}$, $\widehat{\boldsymbol{f}}(\vec{k},t)$ and $f_{j\epsilon\vec{l}\sigma}(t)$ are respectively the Fourier and wavelet expansion coefficients, and $\boldsymbol{\psi}_{j\epsilon\vec{l}\sigma}(\vec{x})$ is wavelet base function. Wavelet indices and their physical implications are explained in Ref. [10]. The scale index of wavelet j takes values of 0, ..., 8 because the number of grid points is 512^3. The wave number range of each wavelet function is $\frac{1}{3}2^j \le k \le \frac{4\sqrt{3}}{3}2^j$.

3. Fourier Analysis Results

Normalized Fourier energy spectra of the velocity and magnetic fields for these three snapshots are shown in

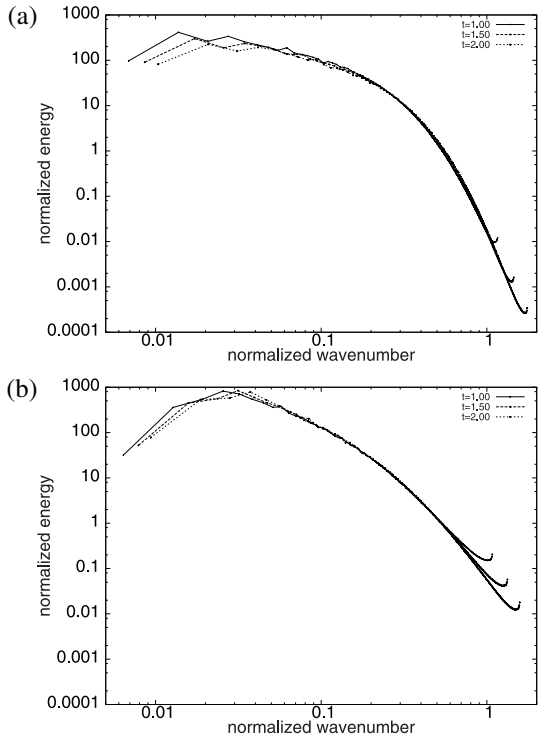

Fig. 1 Normalized Fourier spectra of (a) kinetic and (b) magnetic energies.

Table 1 Dissipation rate of velocity (u) and magnetic (b) fields and their corresponding characteristic wave numbers.

t	$\epsilon^{(u)}$	$\epsilon^{(b)}$	$k_\eta^{(u)}$	$k_\eta^{(b)}$
1.0	0.448	0.601	145.5	156.6
1.5	0.183	0.260	116.3	127.0
2.0	0.086	0.131	96.4	107.1

Fig. 1. To compare the various time results, all the abscissas and ordinates of Fourier spectra were made dimensionless by using the diffusion coefficient and the dissipation rate of the field, i.e., ν and $\epsilon^{(u)}(t) := -\nu\int \boldsymbol{u}(t)\cdot\nabla^2\boldsymbol{u}(t)\mathrm{d}^3\vec{x}$ for the velocity field, and η and $\epsilon^{(b)}(t) := -\eta\int \boldsymbol{b}(t)\cdot\nabla^2\boldsymbol{b}(t)\mathrm{d}^3\vec{x}$ for the magnetic field, respectively. In Table 1 the dissipation rate and the corresponding characteristic wave numbers $k_\eta^{(u)}(t) := \sqrt[4]{\epsilon^{(u)}(t)/\nu^3}$, $k_\eta^{(b)}(t) := \sqrt[4]{\epsilon^{(b)}(t)/\eta^3}$ are listed.

It is remarkable that the functional forms of the normalized energy spectra agree well with each other for each field; that is, the obtained numerical solution is in a self-similar state. This agreement implies that these fully developed turbulent HMHD fields are in the universal equilibrium state. Thus, it is expected that energy transfer contains some universal features of dissipation range dynamics.

It should be noted that the magnetic energy spectra peaks occured around $k/k_\eta^{(b)} \simeq 0.03$ (i.e., $k = 4$). Fourier components lower than these modes do not tend to develop, and significant peaks are not observed for the kinetic energy spectra. These results imply that the forma-

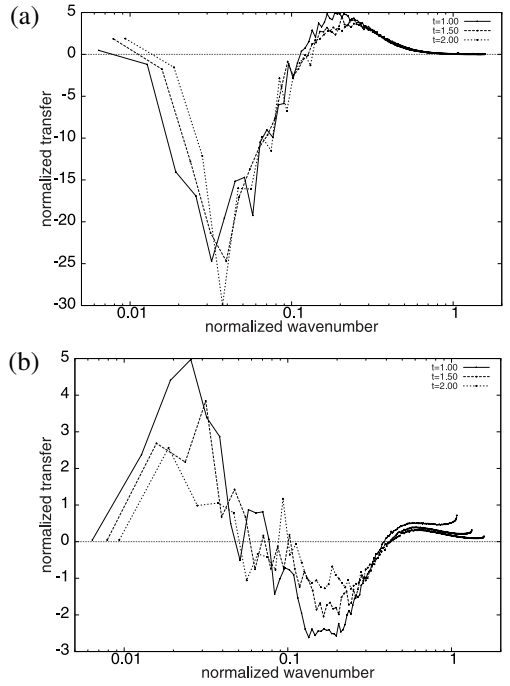

Fig. 2 Normalized Fourier spectra of transfer functions of (a) the magnetic induction term (b) the Hall term.

tion of large-scale structures is rather limited for the magnetic field, compared with that of the velocity field.

Figure 2 shows Fourier spectra of energy transfer by the induction term $T_{\rm Ind}(k,t)$ and the Hall term $T_{\rm Hall}(k,t)$, which are respectively defined as

$$T_{\rm Ind}(k,t) := \sum_{\lfloor|\vec{k}|\rfloor=k} \int_{\vec{x}} \nabla\times(\boldsymbol{u}\times\boldsymbol{b})\cdot\boldsymbol{b}(\vec{k};\vec{x},t)\,\mathrm{d}^3\vec{x}, \tag{6}$$

$$T_{\rm Hall}(k,t) := -\epsilon \sum_{\lfloor|\vec{k}|\rfloor=k} \int_{\vec{x}} \nabla\times(\boldsymbol{j}\times\boldsymbol{b})\cdot\boldsymbol{b}(\vec{k};\vec{x},t)\,\mathrm{d}^3\vec{x}. \tag{7}$$

As is discussed in Ref. [11], we evaluate the energy exchange between the velocity and magnetic fields in terms of $\nabla\times(\boldsymbol{u}\times\boldsymbol{b})$ or $\boldsymbol{j}\times\boldsymbol{b}$, rather than $(\boldsymbol{b}\cdot\nabla)\boldsymbol{u}$ or $(\boldsymbol{b}\cdot\nabla)\boldsymbol{b}$, because of the invariance under the arbitrary change in coordinate system. It should be noted that in Fig. 2 the abscissas and ordinates of the spectra are made dimensionless by $k_\eta^{(b)}$ and $T_\eta^{(b)}(t) := (\eta\epsilon^{(b)}(t))^{3/4}$. Owing to this normalization, the amplitudes of spectra become comparable for different periods, which allow easy estimation of the relative contribution of each term to the dynamics. This implies that the amplitude of the mode interaction term is mainly determined by the dissipation rate of the magnetic field.

Each transfer spectrum has a commom trend in these three snapshots. For the wavenumber $k/k_\eta^{(b)} \lesssim 0.2$, all the transfer spectra show somewhat fluctuating features. The amplitude of energy transfer by the Hall term effect $T_{\rm Hall}(k)/T_\eta^{(b)}$ is relatively smaller than that of energy transfer by magnetic induction $T_{\rm Ind}(k)/T_\eta^{(b)}$ by a factor of one-fifth.

Both forward and backward energy transfers by the Hall term effect are observed for all analyzed datasets (see Fig. 2 (b)). Energy is absorbed around $k/k_\eta^{(b)} \simeq 0.2$ and transferred to the smaller wave number region $k/k_\eta^{(b)} \lesssim 0.1$ and the larger region $k/k_\eta^{(b)} > 0.4$. These wave number ranges of energy loss/acquisition by the Hall term effect are rather stable against the time development, while the modulus of the transfer decreases.

Two interesting features can be obsereved. First, the peak wave number of energy absorbed by the Hall term effect ($k/k_\eta^{(b)} \simeq 0.2$) corresponds to the peak of energy acquired by magnetic induction. Conversely, the peak wave number of energy acquired by the Hall term effect ($k/k_\eta^{(b)} \simeq 0.04$) corresponds to the wave number region in which the magnetic field loses its energy by induction (see Figs. 2 (a) and (b)). This implies that magnetic induction and the Hall term effect contribute to energy transfer in an opposite manner for $k/k_\eta^{(b)} \lesssim 0.2$. That is, the Hall term suppresses forward transfer of the magnetic energy.

Second, the peak of inverse transfer remains near $k/k_\eta^{(b)} \simeq 0.03$, while energy transfer to the largest scale ($k = 1$) remains almost zero (see Fig. 2 (b)). This tendency is consistent with the fact that, the peaks of the magnetic energy spectrum are fixed around $k/k_\eta^{(b)} \simeq 0.03$ and the larger scale components of the magnetic field do not tend to be excited (see Fig. 1), compared with those of the kinetic energy spectrum. This observation suggests that inverse energy transfer by the Hall term effect substantially differs in nature from the so-called inverse cascade of the two-dimensional turbulence of a neutral fluid, which is characterized by spontaneous formation of larger-scale coherent structures [12].

For the two-dimensional turbulence of a neutral fluid, known as Fijortoft's theorem, conservation of energy and enstrophy in the inviscid limit strongly constrain the transfer process [13]. For the HMHD case, such strong constraint relations have not yet been determined, although the system has three quadratic constants in the dissipationless limit: energy, helicity, and hybrid helicity [14].

The tendency of energy transfer of the entire system should be noted. Figure 3 shows Fourier spectra of energy transfers for magnetic and kinetic energies that are respectively defined by

$$T_b(k,t) := \sum_{\lfloor|\vec{k}|\rfloor=k} \int_{\vec{x}} \Big(\nabla\times((\boldsymbol{u}-\epsilon\boldsymbol{j})\times\boldsymbol{b})\Big)\cdot\boldsymbol{b}(\vec{k};\vec{x},t)\,\mathrm{d}^3\vec{x}, \tag{8}$$

$$T_u(k,t) := \sum_{\lfloor|\vec{k}|\rfloor=k} \int_{\vec{x}} \Big(-(\boldsymbol{u}\cdot\nabla)\boldsymbol{u}+\boldsymbol{j}\times\boldsymbol{b}\Big)\cdot\boldsymbol{b}(\vec{k};\vec{x},t)\,\mathrm{d}^3\vec{x}. \tag{9}$$

The abscissas and ordinates of the spectra are made dimensionless by $k_\eta^{(b)}$ and $T_\eta^{(b)}(t)$. Energy is mainly transferred from larger scales to smaller scales as a whole, although weak inverse transfer of the magnetic energy is observed for small wave numbers (Fig. 3 (a)). That is, the contribution of inverse energy transfer due to the Hall term effect to the whole transfer is rather small.

It is interesting to note that the normalized magnetic

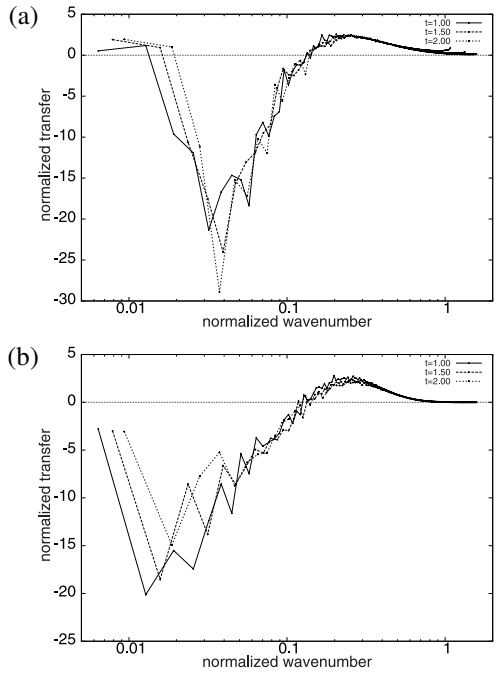

Fig. 3 Normalized Fourier spectra of transfer functions for (a) magnetic and (b) kinetic energies.

energy transfer function $T_b(t)/T_\eta^{(b)}(t)$ is almost stationary (Fig. 3 (a)), while the amplitudes of magnetic induction and the Hall term effect gradually reduce (Figs. 2 (a) and (b)). This implies that forward transfer due to magnetic induction is remarkably compensated by inverse transfer due to the Hall term effect so that the magnetic energy is transferred to the smaller scales in a self-similar manner on the whole. Thus, it is conjectured that inverse energy transfer due to the Hall term effect does not favor the inverse cascade process of the two-dimensional hydrodynamic turbulence, but instead works as a type of regulating process that retains the whole magnetic energy transfer process in a self-similar state.

4. Wavelet Analysis Results

We confirmed that backward transfer due to the Hall term effect is not affected by external forcing such as intrinsic to spontaneous HMHD dynamics. The next step is to determine the type of mode interaction relevant to this inverse transfer process.

To analyze the details of the mode interaction between the different scales of the magnetic field, we introduced the wavelet-scale triad interaction given by the following integral of wavelet modes:

$$\langle \boldsymbol{b}_k | \boldsymbol{b}_m | \boldsymbol{b}_j \rangle_{\rm Hall} := -\epsilon \int \boldsymbol{b}_k \cdot \nabla \times (\boldsymbol{j}_j \times \boldsymbol{b}_m)\, {\rm d}^3\vec{x}. \quad (10)$$

This integral is the wavelet counterpart of the triad interaction analysis of the Fourier modes. In the following equation, the fields $\langle \boldsymbol{b}_k|$, $|\boldsymbol{b}_m|$, and $|\boldsymbol{b}_j\rangle$ are known as to-mode, by-mode, and from-mode, respectively, because the integral implies the rate of change of such energy that is supplied *from* $E_j := \frac{1}{2}\int |\boldsymbol{b}_j|^2 {\rm d}^3\vec{x}$, *to* E_k, *by* the aid of $\boldsymbol{b}_m$, is not directly relevant to the change of E_m.

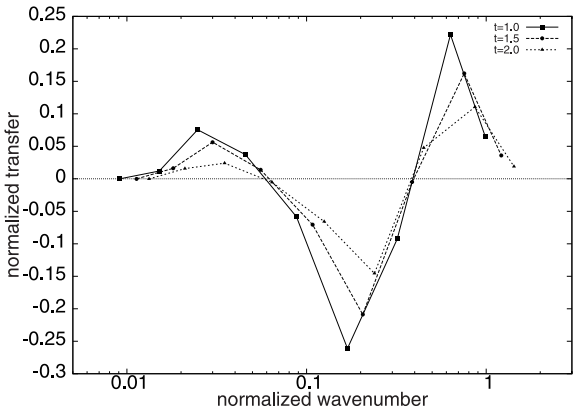

Fig. 4 Normalized wavelet-scale spectra of the Hall term effect $\langle \boldsymbol{b}_k | \boldsymbol{b} | \boldsymbol{b} \rangle_{\rm Hall}$. Ordinates are normalized by the magnetic dissipation rate $\epsilon^{(b)}$.

In Fig. 4, we show the wavelet scale spectra of the Hall term effect defined by $\langle \boldsymbol{b}_k | \boldsymbol{b} | \boldsymbol{b} \rangle_{\rm Hall} = \sum_m \sum_j \langle \boldsymbol{b}_k | \boldsymbol{b}_m | \boldsymbol{b}_j \rangle_{\rm Hall}$. Abscissas are given by $k_j^{(b)}/k_\eta^{(b)}$ where $k_j^{(b)}$ is a characteristic wave number defined by

$$k_j^{(b)} := \sqrt{\int |\nabla \times \boldsymbol{b}_j|^2 {\rm d}^3\vec{x} \Big/ \int |\boldsymbol{b}_j|^2 {\rm d}^3\vec{x}}\,. \quad (11)$$

This spectrum is the wavelet counterpart of transfer function spectrum $T_{\rm Hall}(k)$ given in Fig. 2 (b). As can be observed in the figure, transfer spectra take their extrema at the wavelet resolution classes $k = 2$, 5, and 7. It is interesting to note that the values of the wavelet spectra are positive for $k_j^{(b)}/k_\eta^{(b)} < 0.06$, $0.4 < k_j^{(b)}/k_\eta^{(b)}$ and negative for $0.06 < k_j^{(b)}/k_\eta^{(b)} < 0.4$. In addition, the boundary values appear robust against the time development although each wave number $k_j/k_\eta^{(b)}$ varies in time.

Although energy transfer is local relative to spatial scales, mode interactions that contribute to transfer processes are not necessarily dominated by local triad interactions [15, 16]. To identify the mode interaction relevant to the transfer process, we decomposed the wavelet transfer spectrum into wavelet-scale triad interactions $\langle \boldsymbol{b}_k | \boldsymbol{b}_m | \boldsymbol{b}_j \rangle_{\rm Hall}$.

Figure 5 shows the *j*-*m* plot of the typical wavelet-scale triad interaction profiles for the assigned scales ($k = 2$, 5, 7). The to-mode scales were chosen according to the extrema of the wavelet-scale transfer for $t = 1.0$. While the $k = 5$ wavelet mode corresponds to the scale with the most energy loss, those with $k = 2$ ($k = 7$) correspond to that with the highest energy gain in the smaller (larger) wave number side.

It is remarkable to note that the tendency of energy transfer due to the Hall term effect qualitatively changes at the intermediate scales.

For a larger scale ($k = 2$, Fig. 5 (a)), intense positive

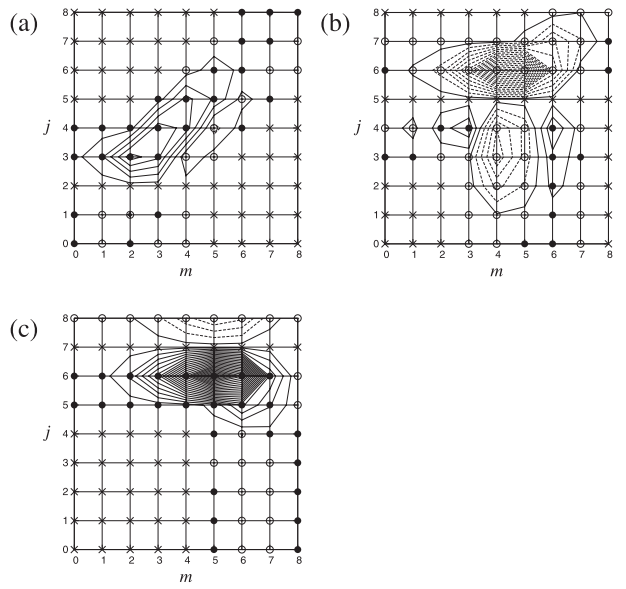

Fig. 5 Typical wavelet-scale triad interaction profiles caused by the Hall term effect $\langle \boldsymbol{b}_k | \boldsymbol{b}_m | \boldsymbol{b}_j \rangle_{\mathrm{Hall}}$ at the time $t = 1.0$ for (a) large ($k = 2$), (b) intermediate ($k = 5$) and (c) small ($k = 7$) spatial scale components. Solid symbols $\langle \boldsymbol{b}_k | \boldsymbol{b}_m | \boldsymbol{b}_j \rangle_{\mathrm{Hall}} > 0$, open symbols $\langle \boldsymbol{b}_k | \boldsymbol{b}_m | \boldsymbol{b}_j \rangle_{\mathrm{Hall}} < 0$, and cross symbols $\langle \boldsymbol{b}_k | \boldsymbol{b}_m | \boldsymbol{b}_j \rangle_{\mathrm{Hall}} = 0$. Contours with increments set to $0.004\epsilon^{(b)}$ are drawn to grasp the amplitudes of interactions.

interactions were aligned in a row on the small-scale side of the $j = m$ and $j = m + 1$ lines, associated with the array of the relatively weak negative triad interactions along $j = m - 1$. The energy of this scale is mainly supplied from the smaller scales with indices $j, m \lesssim k + 3$. This result implies that local and nonlocal triad interactions contribute to inverse energy transfer as a whole. Similar inverse energy transfer by nonlocal interactions is also observed for the cases of $k = 1, 3$ and $t = 1.5$ and 2.0.

For a smaller scale ($k = 7$, Fig. 5 (c)), intense positive (negative) energy transfers were sharply aligned on from-modes $j = k - 1$ ($j = k + 1$), and the contribution outside these scales was negligible. This result implies that dominant energy transfer was caused by local triad interactions. For the by-mode, intense transfer aligned in a rather broader range ($3 \le m \le 6$). Therefore, the principal interactions are local along with contributions by somewhat nonlocal components.

For intermediate scales ($k = 5$, Fig. 5 (b)), the features of distribution appeared to be a superposition of those of larger and smaller scales. Both the strong local transfer to the smaller scales ($j = 6$) and the nonlocal transfer to the larger scales ($j = 2, 3, 4$) were observed.

5. Discussion

It is interesting to note that the interaction tendencies of inverse and forward transfers gradually change at the intermediate scale. This suggests that the Hall MHD system contains two types of qualitatively different dynamics separated by the scales of magnetic structures. Further study is needed to elucidate the relation between energy transfer and coherent structures.

In summary, the Hall term effect on magnetic energy transfer was examined by analyzing a freely decaying turbulent solution that exhibited self-similar spectra such that it was regarded as a universal equilibrium state. Both forward and inverse energy transfers were observed. The spatial scales and the relevant mode interactions are substantially different. The forward transfer occurred at small scales and was dominated by local interactions, while the inverse transfer showed nonlocal interaction features that supplied the magnetic energy to larger scales. Because the solution exhibited universal equilibrium characteristics and was not affected by external forcing, it is expected that a similar energy transfer tendency would be detected in case of other parameters.

This work was performed under the auspices of the NIFS Collaboration Research Program (NIFS10KTBS003) and KAKENHI (Grant-in-Aid for Scientific Research(C)) 22540509.

[1] K. Itoh *et al.*, Phys. Plasmas **12**, 062303 (2005).
[2] S.M. Mahajan and Z. Yoshida, Phys. Plasmas **7**, 635 (2000).
[3] S. Balbus and C. Terquem, Astrophys. J. **552**, 235 (2001).
[4] J. Shiraishi, S. Ohsaki and Z. Yoshida, Phys. Plasmas **12**, 092901 (2005).
[5] H. Miura and D. Hori, J. Plasma Fusion Res. Series **8**, 73 (2009).
[6] H. Miura, Plasma Fusion Res. **5**, S2059 (2010).
[7] K. Araki and H. Miura, Plasma Fusion Res. **5**, S2048 (2010).
[8] P.D. Mininni *et al.*, J. Plasma Phys. **73**, 377 (2007).
[9] H. Miura, J. Plasma Fusion Res. Series **9**, 535 (2010).
[10] K. Araki and H. Miura, IUTAM symposium on Computational Physics and New Perspectives in Turbulence, 149 (2008).
[11] K. Araki and H. Miura, J. Plasma Fusion Res. Series **9**, 446 (2010).
[12] J.C. McWilliams, J. Fluid Mech. **146**, 21 (1984).
[13] M. Lesieur, *Turbulence in Fluids*, 3rd Ed., (Kluwer, Dordrecht, 1997).
[14] L. Turner, IEEE Trans. Plasma Sci. **PS-14**, 849 (1986).
[15] J.A. Domaradzki and R.S. Rogallo, Phys. Fluids A **2**, 413 (1990).
[16] K. Kishida *et al.*, Phys. Rev. Lett. **83**, 5487 (1999).